AIP | Journal of Applied Physics

Surface states in template synthesized tin oxide nanoparticles

A. Cabot, J. Arbiol, R. Ferré, J. R. Morante, Fanglin Chen et al.

Citation: J. Appl. Phys. **95**, 2178 (2004); doi: 10.1063/1.1639946
View online: http://dx.doi.org/10.1063/1.1639946
View Table of Contents: http://jap.aip.org/resource/1/JAPIAU/v95/i4
Published by the American Institute of Physics.

Surface states in template synthesized tin oxide nanoparticles

A. Cabot,[a] J. Arbiol, R. Ferré, and J. R. Morante
EME, Universitat de Barcelona, C/ Martí i Franquès 1, E-08028 Barcelona, Spain

Fanglin Chen and Meilin Liu
School of Material Science and Engineering, Georgia Institute of Technology, Atlanta, Georgia 30332-0245

(Received 23 June 2003; accepted 14 November 2003)

Tin–oxide nanoparticles with controlled narrow size distributions are synthesized while physically encapsulated inside silica mesoporous templates. By means of ultraviolet-visible spectroscopy, a redshift of the optical absorbance edge is observed. Photoluminescence measurements corroborate the existence of an optical transition at 3.2 eV. The associated band of states in the semiconductor gap is present even on template-synthesized nanopowders calcined at 800 °C, which contrasts with the evolution of the gap states measured on materials obtained by other methods. The gap states are thus considered to be surface localized, disappearing with surface faceting or being hidden by the surface-to-bulk ratio decrease. © *2004 American Institute of Physics.* [DOI: 10.1063/1.1639946]

Optoelectronic and gas sensing applications has stimulated an intensive exploration of the electronic structure of tin–oxide surfaces. These studies are usually focused on nearly perfect surfaces, being not always correlated with those features of the functional nanocrystalline materials. SnO_2 has a direct gap at 3.6 eV. Interstitial tin introduces donor levels inside the conduction band,[1] while bulk oxygen vacancies have associated two donor states, experimentally localized at 30 and 150 meV from the bottom of the conduction band.[2] Multivalence of tin makes both defects unusually stable. For small enough particles, a quantum confinement of excitons should take place shifting the absorbance edge to higher energies.[3] On the other hand, for degenerated materials, a blueshift given by the Burstein–Moss theory is also to be expected. However, for nondegenerated tin–oxide nanopowders with particle size between 2 and 20 nm a redshift of the absorbance band edge has already been reported.[4–6] This has been associated with structural defect, and concretely to oxygen vacancies. Nevertheless no evidence has been given for such an assignation.

In this work we report our results on the characterization of tin–oxide nanoparticles synthesized and stabilized while encapsulated inside mesoporous silica structures. Such a physical corseting avoids large particle formation, coalescence, and agglomeration, while allowing the structure stabilization and incorporating oxygen into the lattice.[7] Optical, chemical and electrical properties of thus obtained nanostructures have been examined by means of ultraviolet-visible (UV-vis) diffuse reflectance, x-ray photoelectron spectroscopy (XPS), and conductance measurements.

SnO_2 nanoparticles were obtained from the dissociation of tin–nitrate inside silica mesoporous frameworks.[7] The templates used were SBA-15 structures stabilized at 550 °C. The nitrate compound was introduced in different successive steps by impregnation of the silica with an aqueous solution of tin–oxalate and nitric acid at a 1:3 molar ratio. The precursor material was calcined at different temperatures from 500 to 800 °C for 4 h. Posterior to the calcination, the unsupported powders were collected by dissolving the silica template by means of multiple washing steps with 1 M sodium hydroxide solution in de-ionized water and ethanol at a 1:1 ratio. Once the silica template had been removed, a second firing of the material at 500 °C for 2 h was performed in order to ensure stabilization of the unsupported material and to eliminate residual impurities originated on the template dissolution.

For comparison, a commercial tin–oxide powder (Alfa-Aeasar) with non-nanometric particle size was also considered and here will be referred to as the reference material. At the same time, a third set of tin–oxide nanopowders was obtained precipitating a tin–chloride by the dropwise addition of a 0.1 M ammonia solution. The precipitated compound was thoroughly washed with bidistilled water, dried at 80 °C, and afterwards stabilized by thermal treatment at temperatures from 450 to 1000 °C during 8 h. The crystal size distribution of these materials was determined by transmission electron microscopy (TEM) to be centered at around 10, 40, 55, and 100 nm for the powders calcined at 450, 600, 800, and 1000 °C, respectively. These materials will be here referred to as the precipitated ones.

Nitrogen adsorption/desorption isotherms at 77 K were obtained by a Coulter SA 3100 instrument. The pore-size distribution was calculated using the Barrett–Joyner–Halenda (BJH) method.[8] XPS spectra were obtained on a Physical Electronics 5500 spectrometer, using monochromated Al $K\alpha$ radiation. To minimize discrepancies due to the differences in the powder compactness, the amount of material, possible charging effects and contact resistance, all the measurement conditions and parameters were verified to get the C $1s$ core level of the adventitious carbon at 284.8 eV. Diffuse reflectance (R) UV-vis spectra of the powders were recorded at ambient atmosphere and temperature on a Shimadzu UV-2101PC spectrophotometer equipped with an integrating sphere, using $BaSO_4$ as reference. The spectra were transformed to a magnitude proportional to the extinction coefficient through the Kubelka–Munk absorption function $F(R)$ [$F(R)=(1-R)^2/(2R)$].[9] Photoluminescence (PL)

[a]Author to whom correspondence should be addressed; electronic mail: acabot@el.ub.es

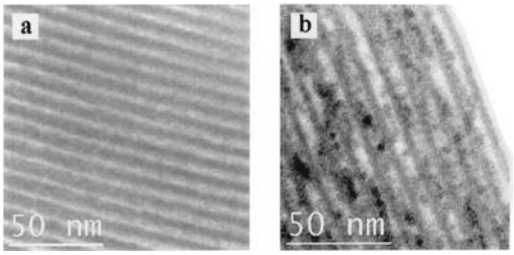

FIG. 1. TEM micrographs of: (a) the SBA-15 template structure and (b) the tin–oxide nanoparticles inside the channels of the mesoporous silica.

measurements were performed using a 30 mW He–Cd laser for ultraviolet excitation ($\lambda = 325$ nm). The luminescent emission was analyzed in backscattering mode by a 0.6 m monochromator and detected with a GaAs photomultiplier. To electrically characterize the materials, the powders were printed onto alumina substrates with Pt interdigitated electrodes and heater. Prior to each measurement, sensors were stabilized at 550 °C during several hours under synthetic air.

Figures 1(a) and 1(b) show TEM micrographs of the empty template structure and the encapsulated tin–oxide nanoparticles, respectively. A slight deformation of the template structure is observed for calcination temperatures higher than that of the initial SBA-15 stabilization treatment. This leads to small increases of the mean particle size distributions respect to that of the initial structure. Fitting of the wide angle x-ray diffraction peaks, corresponding to the supported tin–oxide crystals, allows us to calculate, using Scherer's equation, crystallite sizes of 6.4, 7.1, and 8.4 nm, for the materials calcined at 500, 600, and 800 °C, respectively. These values correspond to the tin–oxide materials synthesized inside a silica template having a pore size distribution centered at 7.2 nm, as measured from N_2 sorption isotherms using the BJH method. TEM counting for some of the samples gives slightly larger mean particle sizes, with size distributions having a full width at half maximum around 1.5 nm. No preferential growth direction of the tin–oxide nanoparticles inside the channels is observed.

The valence band of the unsupported template synthesized (TS) nanopowders, as measured by XPS, clearly resembles that of the reference material [Fig. 2(a)]. By this technique, no appreciable differences in the density of gap states are obtained between the different materials. Figure 2(b) shows the XPS spectra corresponding to the O 1*s* core level region. The main band is associated with the lattice oxygen from the SnO_2 structure, while the shoulder at higher energies accounts for adsorbed oxygen-containing species. As expected, the quantity of adsorbed species is larger in the TS tin–oxide than in the reference one, correlating with the much larger surface area of the former. A small positive shift of the spectra corresponding to the TS material is obtained when compared with the reference one. This could, to some extent, stem from a bulk doping effect, but in the greatest part it is considered here to be associated with a decrease of the surface band bending.

Figure 3 shows the UV-vis diffuse reflectance spectra of the different material. The UV-vis spectra of the reference tin–oxide is dominated by the edge associated with the interband electronic transitions. The TS nanopowders show a

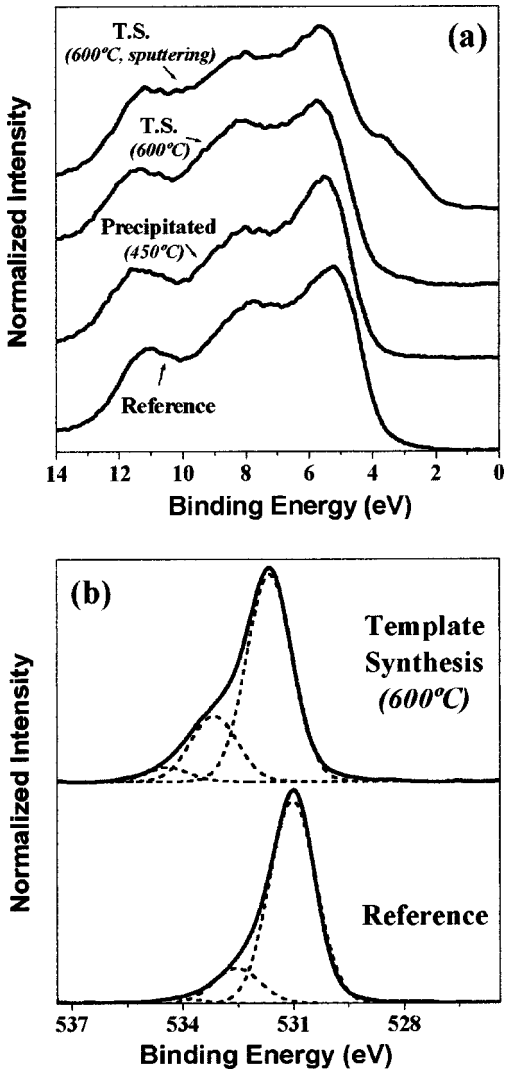

FIG. 2. (a) Valence band region of the XPS spectra from the reference tin–oxide powders, the precipitated material calcined at 450 °C, and the TS calcined at 600 °C. The spectra of the TS nanopowders after a sputtering process with Ar^+ ions is also plotted. (b) O 1*s* core region of the TS nanopowders calcined at 600 °C and that of the reference material. Data points are fitted with Gaussian–Lorentzian functions.

redshift of the absorption edge. The UV-vis spectra of the precipitated material calcined at 450 °C also show a narrowing of the optical band gap. In this case, the shift on the reflectance edge progressively vanishes when stabilizing the material to higher temperatures, recovering the 3.6 eV bandgap value of the reference material after stabilization treatments at high enough temperature. Otherwise, for the TS nanopowders, the redshift of the absorbance edge is maintained after calcination of the encapsulated powders up to 800 °C.

The PL spectra of the tin–oxide have been reported to show a band at 2.2 eV, which was associated with oxygen vacancies.[10] Another band on the PL spectra centered at 3.1 eV has also been reported and determined not to change dramatically with the analysis temperature.[11] However, not a clear idea of its precedence was given. Similar bands are observed for our TS materials (Fig. 3, inset), which we consider to be probably related to the same electron transition as that originating in the UV-vis absorbance band.

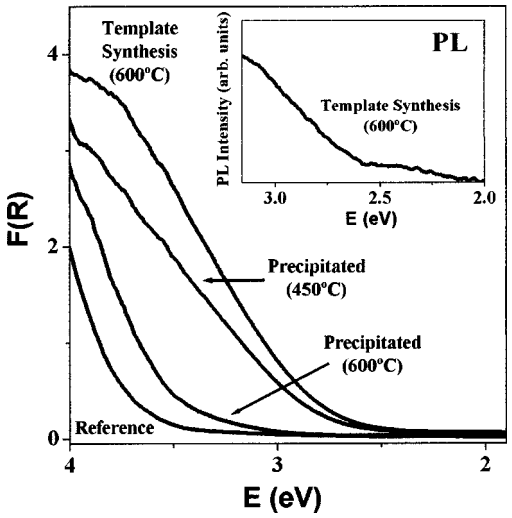

FIG. 3. Diffuse reflectance UV-vis spectra in Kubelka–Munk units. The inset shows the room temperature photoluminescence spectra of the template-synthesized material calcined at 600 °C.

From the literature, oxygen vacancies are the postulated main source of the electron states originating in the band-gap optical transitions. However, the existence of a considerable quantity of oxygen vacancies on the material surface should lead to the apparition of an occupied band of states in the bottom of the band gap,[12] as shown on the XPS valence band of the TS tin–oxide structure after a 1′ Ar^+ ion bombardment. No similar band of states is observed for the TS material before sputtering.

On the other hand, oxygen deficient structures are coupled with an increase of the carrier density. However, the conductivity of the TS materials is not significantly larger than that of the reference or the precipitated materials to account for a substantial amount of oxygen vacancies (Fig. 4). Aside from the charge trapped on intrinsic surface states and defects of the oxide lattice,[13] the temperature dependence of the sensor conductance in a dry air atmosphere is dictated by the temperature ranges of stability of the different ionosorbed oxygen species.[14,15] Differences in the conductance dependence with the temperature, observed between the different samples analyzed here, are related to different surface structures and defect density, which determine the sticking coefficient, coverage, and electrical role of the adsorbed species.

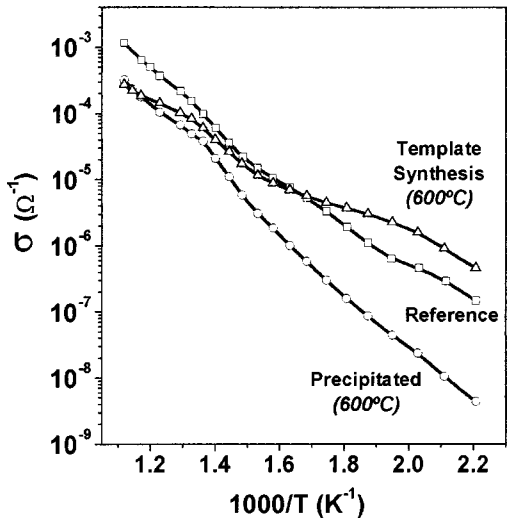

FIG. 4. Dependence of the sensor conductance with the inverse temperature in a synthetic air atmosphere. Data were obtained when increasing material temperature.

We directly associate to the preservation of the small particle size the fact that our TS materials kept the gap states, even when stabilized at 800 °C. The shift of the UV-vis reflectance edge is due to electron transitions taking place between states localized on the surface or the nearest surface layers of the particles. This density of states is associated with the surface disorder or defects on the last layers of the grains, inherent to the small size of the particles.[16] The vanishing of this band after severe calcination treatments in the precipitated nanopowders is directly related to the growth of the tin–oxide crystals, the consequent decrease of the surface-to-bulk ratio, and the surface reconstruction, becoming faceted. The evolution of the UV-vis absorption band with the calcination temperature, in references dealing with materials stabilized at low temperatures,[4,5] may be explained by the combined effect of the material composition, the crystal growth, and the surface reconstruction.

To summarize, tin–oxide nanoparticles synthesized inside mesoporous structures presented a large density of states in the semiconductor gap, shifting the UV-vis absorbance edge to lower energies. The dependence of the density of states on the particle size, and the lack of XPS and electrical evidences of an oxygen deficient structure, leads us to consider these optical transitions to arise from surface localized states. The decrease of the density of gap states with the grain growth thus stems from either the improvement of the defective surface structure inherent to the very small crystallites or from the decrease of the surface-to-bulk ratio. These surface states dictate the material surface–gas interaction, changing the temperature dependence of its conductance in an atmosphere containing oxygen.

[1] Ç. Kiliç and A. Zunger, Phys. Rev. Lett. **88**, 095501 (2002).
[2] S. Samson and C. G. Fonstad, J. Appl. Phys. **44**, 4618 (1973).
[3] N. Chiodini, A. Paleari, D. DiMartino, and G. Spinolo, Appl. Phys. Lett. **81**, 1702 (2002).
[4] N. Sergent, P. Gélin, L. Périer-Camby, H. Praliauda, and G. Thomas, Sens. Actuators B **84**, 176 (2002).
[5] N.-L. Wu, L.-F. Wu, I. A. Rusakova, A. Hamed, and A. P. Litvinchuk, J. Am. Ceram. Soc. **82**, 67 (1999).
[6] D. A. Popescu, J.-M. Herrmann, A. Ensuque, and F. Bozon-Verduraz, Phys. Chem. Chem. Phys. **3**, 2522 (2001).
[7] A. Cabot, J. Arbiol, E. Rossinyol, J. R. Morante, F. Chen, and M. Liu, Electrochem. Solid-State Lett. (in press).
[8] E. P. Barret, L. G. Joyner, and P. P. Halenda, J. Am. Chem. Soc. **73**, 373 (1951).
[9] M. W. Urban, *Vibrational Spectroscopy of Molecules and Macromolecules on Surfaces* (Wiley, New York, 1993), p. 90.
[10] T. Hayakawa, T. Enomoto, and M. Nogami, J. Mater. Res. **17**, 1305 (2002).
[11] T. W. Kim, D. U. Lee, and Y. S. Yoon, J. Appl. Phys. **88**, 3759 (2000).
[12] P. A. Cox, R. G. Edgell, C. Harding, W. R. Patterson, and P. J. Tavener, Surf. Sci. **123**, 179 (1982).
[13] F. Greuter and G. Blatter, Semicond. Sci. Technol. **5**, 111 (1990).
[14] N. Yamazoe, J. Fuchigami, M. Kishikawa, and T. Seiyama, Surf. Sci. **86**, 335 (1979).
[15] S. Chang, J. Vac. Sci. Technol. **17**, 366 (1980).
[16] J. Melsheimer and D. Ziegler, Thin Solid Films **19**, 35 (1985).